

Structural damage in boron carbide under contact loading

D. Ge^{a,b}, V. Domnich^a, T. Juliano^a, E.A. Stach^b, Y. Gogotsi^{a,*}

^a Department of Materials Science and Engineering, A.J. Drexel Nanotechnology Institute, Drexel University, Philadelphia, PA 19104, USA

^b National Center for Electron Microscopy, Lawrence Berkeley National Laboratory, Berkeley, CA 94720, USA

Received 18 March 2004; received in revised form 3 May 2004; accepted 4 May 2004

Available online 1 June 2004

Abstract

A systematic study of mechanical deformation of boron carbide under contact loading is conducted using scratching and depth-sensing indentation (nanoindentation). Both single crystal and polycrystalline materials are investigated by means of Raman microspectroscopy and transmission electron microscopy (TEM). High resolution TEM images of scratch debris reveal various microstructural changes including formation of nanocrystals, as well as lattice shearing and distortion on nanoscale. Deformation bands and microcracks oriented along the (1 1 3) planes are visible in cross-sectional TEM micrographs of indentations. Narrow amorphous bands and local disordered areas are observed in plan-view TEM images. Evidence for a high-pressure amorphous phase is also presented. It is concluded that scratching and nanoindentation change the microstructure of boron carbide in a similar manner. In addition, the evidence for formation of sp^2 hybridized carbon as a result of structural changes induced by contact loading is found by electron energy loss spectroscopy (EELS).

© 2004 Acta Materialia Inc. Published by Elsevier Ltd. All rights reserved.

Keywords: Boron carbide; Scratch test; Nanoindentation; Transmission Electron Microscopy; Raman spectroscopy

1. Introduction

Boron carbide is used for a wide range of engineering applications because of its exceptional hardness, outstanding elastic modulus, and low specific gravity [1]. Given such unique mechanical properties, mechanical deformation of boron carbide under different types of loading conditions has been studied over the past 20 years [2–4]. Various testing methods, including ultrasonic techniques [3] and Vickers indentation [4] were utilized to measure modulus, hardness and fracture toughness. There is considerable interest in the application of boron carbide as light-weight armor [1], and shock compression tests have been performed to investigate its effectiveness against ballistic impact [5–7]. Boron carbide was found to display an anomalous shock-yielding behavior under high-impact shock compression, resulting in catastrophic deformation at high

contact pressures in excess of a certain pressure threshold [8]. In a recent study of shock fragments produced by ballistic testing of hot-pressed boron carbide, Chen et al. [9] suggested that the formation of nanoscale intragranular amorphous bands might be responsible for this phenomenon, as opposed to deformation by twinning when contact pressures associated with ballistic impact are relatively low. Despite these studies, to date the deformation behavior of boron carbide under contact loading is poorly understood. A technique that involves depth-sensing indentation (nanoindentation) and mechanical scratching, combined with Raman microspectroscopy and transmission electron microscopy (TEM), is used in the present study.

Nanoindentation has proven to be a powerful technique in providing information on mechanical properties (hardness or elastic modulus) of the investigated materials, and variation of these properties with penetration depth, based on analysis of respective load–displacement curves [10–13]. While diamond anvil experiments are capable of studying the mechanical deformation and phase transformation in bulk materials

* Corresponding author. Tel.: +1-215-895-6446; fax: +1-215-895-6760.

E-mail address: yg36@drexel.edu (Y. Gogotsi).

under hydrostatic pressure, the material behavior under nanoindentation is of more relevance to realistic contact or impact loading conditions [14]. Average contact pressure during indentation, which is known to scale with the material hardness, reaches 40–45 GPa in boron carbide single crystals [11]. It has been reported that the presence of deviatoric stresses associated with nanoindentation may significantly facilitate high pressure phase transitions, lower their pressure threshold and even change the mechanisms of these transitions [15,16]. At the same time, significant changes in Raman spectra of the indented area compared with those of the pristine material indicated that some drastic structural changes were occurring in boron carbide under localized contact loading [17]. The authors attributed such changes to either a solid state phase transformation (similar to a transition from rhombohedral to orthorhombic structure in boron carbide reported by Manghnani [18]), or to amorphization of the B_4C structure during nanoindentation.

The shape of nanoindentation load–displacement curves can often suggest structural changes that occur within the indented material during the test. For example, the onset for dislocation slip or twinning in Al_2O_3 and SiC [19–22] and the solid-state phase transformations in Si and Ge [23–25] have been associated with discontinuities in nanoindentation load–displacement curves of these materials. However, no such peculiarities have been reported for boron carbide, whose deformation behavior during nanoindentation most closely resembles that of a classical elastoplastic response, with featureless loading and unloading curves and seemingly purely elastic unloading [11].

Although both shock impact tests and nanoindentation established that the mechanical deformation of boron carbide involves some unusual structural changes, the underlying mechanisms responsible for the unique mechanical behavior of this material are not clear. Furthermore, the possibility of a solid-state phase transition in boron carbide under pressure is still to be verified. In this study, cross-sectional and plan-view TEM studies are implemented to investigate the microstructural changes beneath nanoindentation in both single crystal $B_{4.3}C$ samples and hot-pressed polycrystalline boron carbide, and Raman spectroscopy is done inside the indented areas. Results of the investigation of scratches produced on single crystal boron carbide are also reported.

2. Experimental

Single crystal and polycrystalline boron carbide were tested for this study. The single crystal samples were prepared by float zone method at the Advanced Materials Laboratory of the National Institute for Materials

Research in Tsukuba, Japan [17]. The crystal composition was determined to be $B_{4.3}C$ using a carbon determinator (WR-12, Leco Co., USA). The polycrystalline materials were hot-pressed at Wacker Ceramics, Germany. The surfaces of both materials were polished using first 3 μm and then 1 μm diamond abrasive.

Nanoindentation experiments were performed using a Nano Indenter XP[®] (MTS) equipped with a Berkovich diamond indenter. The maximum applied loads ranged from 100 to 200 mN. The loading and unloading rates varied between about 6 and 13 mN/s. Post-indentation characterization was performed using a Renishaw 1000 Raman spectrometer (Renishaw, UK). An argon ion laser operating at the excitation wavelength of 514.5 nm was used for Raman analysis. Cross-sectional TEM (XTEM) specimens of single crystal $B_{4.3}C$ were prepared by the lift-out technique using a dual-beam focused ion beam (FIB) station (FEI Strata DB 235). A low dose of Ga^+ ion beam (~ 70 pA) was adopted in the final cleaning cut to minimize surface damage and redeposition. The plan view TEM samples were extracted from indented hot-pressed polycrystalline material. Preparing plan-view TEM specimens without introducing any micro-structural changes in the indentation area involves considerable experimental challenges [26,27], especially for an extremely hard and brittle material such as boron carbide. The preparation of plan-view TEM samples starts with two lines of nanoindentations that cross in an “+” shape on a polished surface of polycrystalline boron carbide. The spacing between indentations was 10 μm . The indented specimen was then thinned down to 100 μm by mechanical polishing. After dimpling, a layer of nail polish was applied to protect the indentation surface from redeposition during single-side ion milling. Interrupted ion milling was used to minimize heating and possible structural changes in a Gatan precision ion polishing system (PIPS) station. Raman spectroscopy was performed on both cross-sectional and plan-view samples before and after sample preparation. Spectra taken at each time showed identical peak intensities and positions (see Fig. 6 in Appendix A), suggesting no structural change during the sample preparation. The TEM samples were examined in a JEOL 2010F TEM operating at 200 kV with a point-to-point resolution of 0.23 nm and a lattice resolution of 0.10 nm. A Gatan image filter was also attached for energy filtered imaging and electron energy loss spectroscopy (EELS).

Mechanical scratches on the polished surface of a single crystal sample were made using a diamond scriber. The scratch grooves and debris were characterized by Raman spectroscopy. Scattered debris was collected onto a lacey carbon coated grid for TEM examination. The advantages of TEM analysis on wear debris include easy collection and exclusion of any possible artifacts due to sample preparation.

In situ nanoindentation in a JEOL 3010 TEM was performed to image the microstructural evolution under indentation in real time by using a recently developed *in situ* stage [28]. During in situ nanoindentation, a Berkovich diamond indenter approaches the electron-transparent sample in the normal direction of electron beam. Penetration of the diamond indenter into the edge of the sample is controlled by a piezoceramic actuator, along the $\langle 001 \rangle$ zone axis of the single crystal. The sample is a 500-nm thick membrane that was prepared at one edge of a thin slice of single crystal $B_{4.3}C$ by using a dual-beam FIB.

3. Results and discussion

3.1. Raman analysis

Consistent with previously reported data [29–32], Raman spectra of samples prior to contact loading showed a series of bands extending from 200 to 1200 cm^{-1} (Fig. 1(a)), assigned in literature to vibrations of principal structural elements in boron carbide, icosahedra and three-atom linear chains [29–32]. Examination of Raman spectra obtained from various surfaces subjected to contact loading (Figs. 1(b)–(d)) reveals drastic structural changes that occur in boron carbide during indentation or scratching. The most notable is the appearance of several new broad bands at higher frequencies, in particular a prominent band centered around 1330 cm^{-1} . Such changes in Raman spectra are consistent with previous observations of Berkovich nanoindentations made in boron carbide single crystals [17]. As one of the possible deformation scenarios, it was

suggested in earlier work that extreme disordering of boron carbide during nanoindentation might lead to the destruction of the B_4C structure and formation of carbon rings, possibly incorporating some boron, from the broken C–B bonds. An alternative scenario included the possibility of a high pressure solid-state phase transformation in material under the indenter [17]. Since Raman spectra have similar high-frequency bands for indents made in single crystals (Fig. 1(b)) and polycrystalline (Fig. 1(c)) material, as well as for scratches and scratch debris (Fig. 1(d)), a similarity in microstructural changes in the material under various contact loading situations is evidenced. Additionally, spectra reported in Fig. 1(b)–(d) have been acquired using a low intensity laser beam in order to avoid artifacts due to laser heating. When an intense laser beam was used for investigation of scratch debris, increased temperature on the analyzed surfaces resulted in the appearance of characteristic features of amorphous or disordered sp^2 carbon, as evidenced by Raman bands at 1350 and 1590 cm^{-1} (the D and G bands [33]) in Fig. 1(e). This observation also indirectly confirms that the structure after scratching or nanoindentation testing is not merely sp^2 carbon, albeit a wide variation of spectral features that different forms of carbon can encompass [34]. In order to explore the mechanisms responsible for fundamental changes in Raman spectra of boron carbide and to understand the details of its deformation behavior under contact loading, TEM investigation of both scratch debris and indentations was employed.

3.2. TEM results and analysis

TEM investigation of boron carbide began with analysis of debris from scratches made in single crystal samples. The debris particle sizes were on the nanometer to micrometer scale. A relatively small debris particle of about 200 nm in diameter is shown in Fig. 2. Although the low-magnification image (Fig. 2(a)) did not give any hints on the structural changes in boron carbide after scratching, an abundance of interesting features was revealed from the high-magnification images of the debris edge (Figs. 2(b)–(d)). In particular, high-magnification images suggest that during dynamic loading, single crystal boron carbide can experience various deformation paths which include formation of nanocrystals (Fig. 2(b)), lattice shearing (Fig. 2(c)), and lattice deflection (Fig. 2(d)). A preferred orientation for the nanocrystalline grains in Fig. 2(b) was not observed. Only two plausible mechanisms may be responsible for such random grain orientation: (i) the single crystal has been deformed via breakage of some lattice bonds and subsequent rotation has occurred in order to accommodate shear strains, or (ii) boron carbide underwent a solid-state phase transformation under high contact pressures, and the resultant high-pressure phase

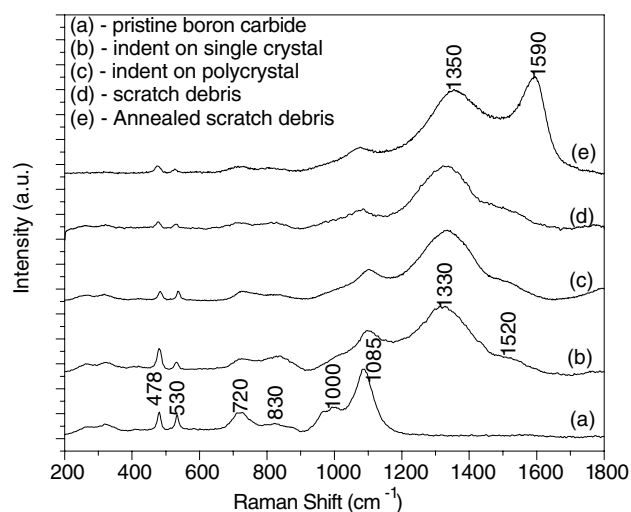


Fig. 1. Raman spectra of: (a) pristine single crystal $B_{4.3}C$; (b) indented single crystal; (c) indented hot-pressed polycrystal; (d) scratch debris of a single crystal; (e) annealed scratch debris in air by using an argon ion laser with excitation wavelength of 514.5 nm .

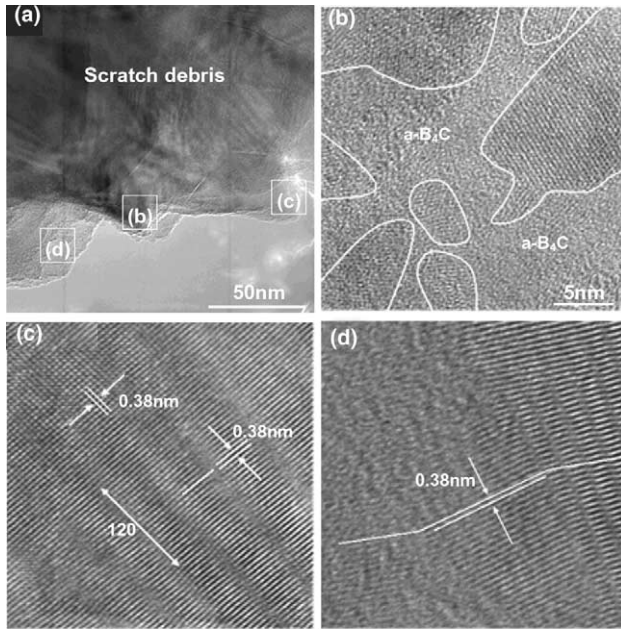


Fig. 2. (a) TEM micrograph of scratch debris. (b)–(d) Magnified images of the debris edge area, corresponding to the boxed area in (a).

recovered to the regular rhombohedral structure after load release, in the form of randomly oriented nanocrystalline grains. The lattice shearing observed in Fig. 2(c) occurred along a specific crystallographic plane of single crystal $B_{4.3}C$, namely the $(1\ 2\ 0)$ plane, and the resultant planar defects resemble shear induced amorphous bands similar to those observed by Chen et al. [9] in the boron carbide ballistic fragments. We also note that our comparative energy dispersive spectroscopy (EDS) analysis of scratch debris and the pristine material did not show any noticeable changes in the boron-to-carbon ratio, nor did it show the presence of oxygen.

XTEM of a 200 mN indentation produced on the $(00\ 1)$ surface of single crystal $B_{4.3}C$ is shown in Fig. 3. The bright field micrograph of a typical indentation (Fig. 3(a)) reveals shear bands oriented along the $\langle 1\ 1\ 3 \rangle$ direction, which is in contrast to the twinning habit planes along the $\langle 1\ 1\ 0 \rangle$ direction observed in hot-pressed boron carbide. This is a clear example of a slip mechanism, which apparently proceeded through the creation and propagation of microcracks. Using selected area diffraction (SAD), no evident signs of a phase transformation or amorphization beneath the indent were observed. However, when the specimen was tilted to the $\langle 3\ 1\ \bar{1} \rangle$ zone axis of the parent material, the electron diffraction of the indented area produced a very peculiar pattern shown as an inset in the right bottom corner in Fig. 3(b). This pattern consists of two sets of diffraction patterns with the series of $(1\ \bar{1}\ 2)$ planes as the common reflections, one of which is the same as the diffraction pattern of the surrounding pristine area (inset in the left top corner in Fig. 3(b)), and the other can be assigned to

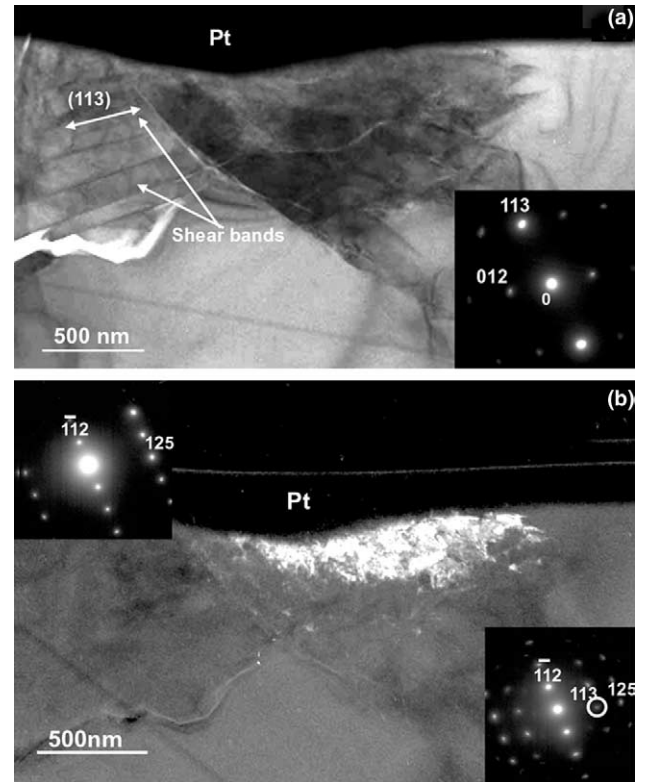


Fig. 3. (a) Bright field and (b) dark field XTEM micrographs of a 200 mN indent.

the zone axis of the $\langle 5\ 1\ \bar{2} \rangle$ direction of the rhombohedral structure. This indicates that some part of the indented material has been rotated around the $\langle 1\ \bar{1}\ 2 \rangle$ direction by about 7.5° . By choosing the $(1\ 1\ 3)$ reflection (see Fig. 3(b) inset), the rotated part has been highlighted in the dark field image shown in Fig. 3(b). It is evident that the highlighted part of the indent has a polycrystalline state (Fig. 3(b)), with the size of the smallest grains on the order of 20 nm. Thus, single crystal boron carbide was broken under load into nanocrystals which rotated to a certain degree under indenter. The structural changes within the indented area are also quite heterogeneous. Because the appearance of deformation bands and microcracks greatly relaxed the elastic strain on the left side beneath the indent shown in Fig. 3, lattice rotation and nanocrystallization was probably constrained in the unrelaxed side of the indent (the bright area in the indented region in Fig. 3(b)). In addition, the appearance of shear bands and their glide into deeper areas under a penetrating Berkovich diamond tip was videotaped in real-time during *in situ* nanoindentation on a thin membrane of bulk single crystal $B_{4.3}C$. The movement of strong bend contours was also observed around the affected region. However, corresponding pictures are not included in this publication due to a low video resolution.

Fig. 4 shows the high resolution images obtained in the plan view TEM investigation of a 100 mN inden-

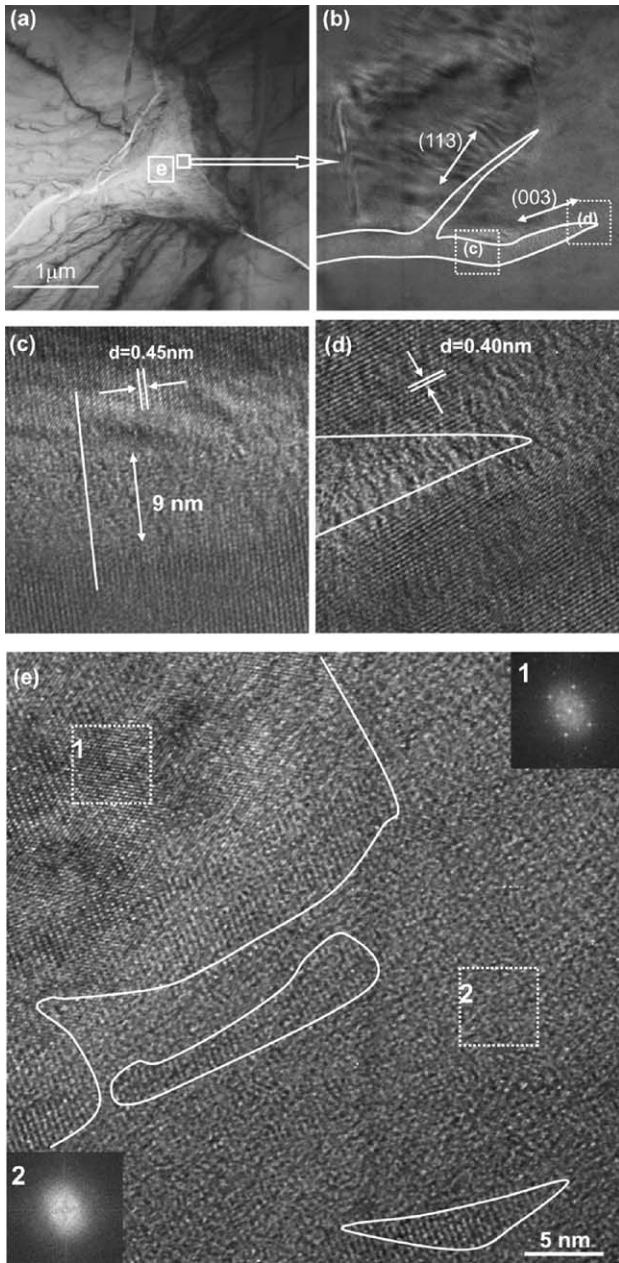


Fig. 4. (a) Plan view TEM micrograph of a 100 mN Berkovich indent. (b) A magnified image showing the amorphous bands along the (113) and (003) planes. (c) and (d) HR lattice images corresponding to the boxed area in (a) and (b). (e) A primarily amorphous region within the Berkovich indent.

tation made in hot-pressed boron carbide. The surface cracks oriented along certain crystallographic directions were found at the corner and along the edge of the indent (Fig. 4(a)). Although SAD of the entire indent did not show signs of amorphization or phase transformation, the magnified images in Figs. 4(b) and (c) reveal narrow amorphous bands (up to ~ 9 nm) within the indentation area, similar to amorphous bands (~ 1 – 3 nm wide) observed by Chen et al. [9] in small boron carbide fragments collected after high velocity ballistic impact.

The observation of a perfectly aligned lattice on either side of the amorphous bands in Fig. 4(c) rules out the possibility of formation and subsequent rebonding of the two cracked surfaces or local melting under contact pressure. No evidence of extensive dislocation plasticity was observed at the sharp tip of the amorphous bands (Fig. 4(d)). The extremely narrow width and the sharp tip of the amorphous bands suggest that amorphization was initiated by local shear instability. In contrast to the observation of impact fragments in which the amorphous bands were oriented along a specific preferred plane [9], the amorphous bands in the indents have various orientations and intersect with each other to form a network. In the central area of the residual indent, a local amorphized region rather than narrow bands is observed as well. Within the amorphous zone, there are several nano-sized grains with retained orientation (Fig. 4(e)). Fast Fourier transformation (FFT) simulation is employed on the two boxed areas (Box 1, 2) for comparison. The FFT pattern of Box 1 shows spot reflections indicative of the rhombohedral crystal structure of boron carbide. In contrast, only a diffuse halo, a typical feature of amorphous material, is visible in the simulated pattern of Box 2. The observed unsmooth interface between the crystalline and amorphous zones is similar to earlier high resolution observations for silicon [26]. It is conceivable that due to the limited number of dislocation slip systems in boron carbide, anisotropy and a heterogeneous stress distribution beneath the indenter triggers amorphization along the preferred crystallographic directions or a localized distortion-induced disordering.

It is important to note that similar amorphous shear bands were also observed along some crystallographic planes beneath silicon indentations [35,36]. Because silicon is known to experience phase transformations under indentation [37], a possible high-pressure phase transformation during boron carbide indentation has been considered. Manghnani [18] suggested a phase transition from the rhombohedral to orthorhombic structure in boron carbide at a hydrostatic pressure of ~ 20 GPa. The high-pressure phase was reportedly denser and more compressible than the ambient-pressure phase. Moreover, further compression was reportedly followed by another phase transition when the hydrostatic pressure reached 44–49 GPa. However, this observation has not been independently confirmed and the detailed lattice information of the high-pressure phase has never been reported in the literature. In the present TEM observations, both SAD and high resolution imaging showed that some patterns slightly deviated from the calculations based on the published lattice constant for boron carbide (JCPDS-ICCD #35-0798). A small mismatch could be explained by local lattice distortion due to residual strain or that the rhombohedral unit cell volume can vary with the

carbon ratio in this compound [38]. However, many solid-state phase transformations in different materials involve a very small lattice distortion, such as that found in PZT [39] and Si [40]. Additional characterization is required to clarify the existence of a high-pressure phase transformation in boron carbide during contact loading and the precise reason for appearance of new Raman bands.

By means of EELS, it was found that the amorphous structure (boxed area 2 in Fig. 4(e)) showed a different carbon K edge compared to the crystalline lattice (Fig. 5). The appearance of an enhanced π^* peak in the carbon K edge indicates the existence of sp^2 bonding, i.e. carbon double bonding in the material. The change of chemical composition within the indents is not expected because both surface oxidation and bulk diffusion in boron carbide seem unlikely at room temperature. Under contact pressures of ~ 40 GPa achieved during nanoindentation, it is reasonable to conceive that some carbon double bonds have been produced by lattice breaking and rearrangement of carbon atoms. Unlike the carbon edge, the core-loss edge of boron shows little fundamental changes (Fig. 5). Therefore, it is believed that the boron atoms have retained their chemical state, while the chemical state of carbon has been partially modified during nanoindentation. Combining Raman results with TEM observations, the new broad Raman bands of the residual indent can be thus attributed to amorphous boron carbide observed in Fig. 4(e). However, it is noteworthy to mention that this amorphous or disordered phase is different from the amorphous thin film of boron carbide

produced by vapor phase deposition at ambient pressure [41], as suggested by Raman spectra and the changed chemical state of carbon atoms. Thus, this may be a denser high pressure amorphous material produced either as result of direct amorphization or transformation of a metastable high-pressure phase of boron carbide.

4. Conclusions

The microscopic and spectroscopic investigation through Raman analysis combined with TEM showed that similar microstructural changes were induced in boron carbide by scratching and nanoindentation. Raman data show the appearance of new peaks in scratched and indented areas which are wide and indicative of a phase that is amorphous in nature. In the XTEM investigation, the deformation bands were observed along certain crystallographic planes and a heterogeneous deformation was evidenced as well. Plan-view TEM observations have identified the formation of amorphous bands and local amorphized areas in the residual indentations. The EELS results showed that contact loading not only affected the lattice structure of this material but also changed the chemical state of carbon atoms. Therefore, the significant changes in the Raman spectra of boron carbide after contact loading can be attributed to presence of a high-pressure amorphous phase of boron carbide.

Acknowledgements

The authors thank Dr. T. Tanaka of the National Institute for Materials Science in Japan and Dr. K. Schwetz and Dr. A. Rendtel of Wacker Ceramics in Germany for providing the single crystal and polycrystalline materials, respectively. Insightful discussions with Dr. J.W. McCauley of U.S. Army Research Laboratory and Prof. M. Trenary of the University of Illinois at Chicago are greatly appreciated. Thanks are also due for the use of the electron microscopy facilities at the Penn Regional Nanotechnology Facility of the University of Pennsylvania and for access to the FIB station at the Center for Advanced Materials and Nanotechnology of Lehigh University. This work is partially supported by NSF under Grant No. DMR-0196424. The Raman microspectrometer at Drexel University was purchased under NSF Grant No. DMR-0116645. The work at NCEM was supported by the Director, Office of Science, Office of Basic Energy Sciences, Division of Materials Sciences and Engineering, of the US Department of Energy under Contract No. DE-AC03-76SF00098. The authors are also indebted to Dr. A. Minor of NCEM, Lawrence Berkeley National Laboratory for assistance with the *in situ* experiments.

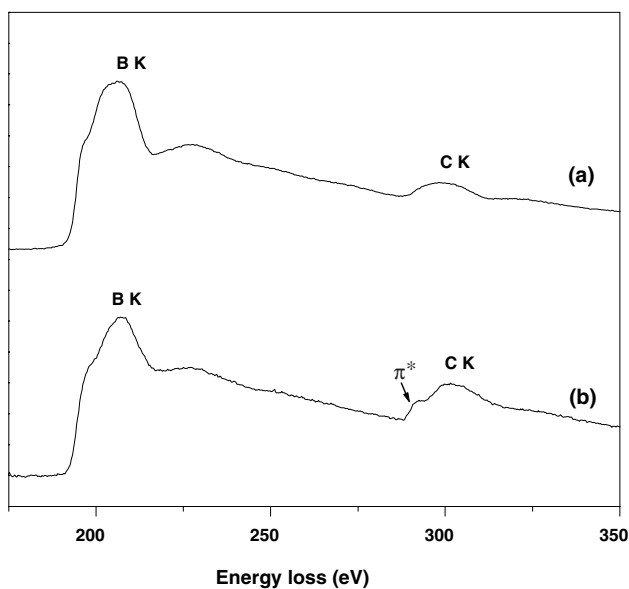


Fig. 5. EELS spectra of: (a) pristine; (b) amorphized boron carbide of box 2 in Fig. 4(e).

Appendix A

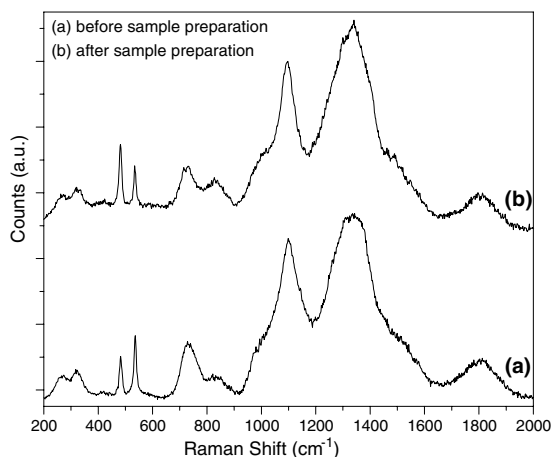


Fig. 6. Raman spectra of a Berkovich indentation on hot-pressed polycrystalline boron carbide (a) before and (b) after sample preparation for TEM investigations. No obvious difference is observed in these two spectra, indicating that the phase composition of the sample has not been altered during ion milling. Similar spectra were collected from all TEM samples before and after sample preparation.

References

- [1] Thevenot F. Boron carbide – a comprehensive review. In: de With G, Terpstra RA, Metselaar R, editors. *Properties of ceramics*, vol. 2. London: Elsevier Applied Science; 1989. p. 2.1.
- [2] Schwetz KA, Lipp A. Boron carbide, boron nitride and metal borides. *Ullmann's encyclopedia of industrial chemistry*, vol. 4A Weinheim: Verlag Chemie; 1985. p. 265.
- [3] Lemis-Petropoulos P, Kapaklis V, Peikrshvili AB, Politis C. *Int J Mod Phys B* 2003;17:2781.
- [4] Lee H, Speyer RF. *J Am Ceram Soc* 2002;85:1291.
- [5] Bartkowski PT, Dattatraya PD, Grove DJ. Spallation of hot pressed boron carbide ceramic. In: Thadhani NN, Horie Y, editors. *Shock compression of condensed matter*. Furnish, MD: American Institute of Physics; 2001. p. 799.
- [6] Blumenthal WR, Gray GTI. Characterization of shock-loaded aluminum-infiltrated boron carbide cermets. In: Schmidt SC, Johnson JN, Davison IW, editors. *Shock compression of condensed matter*. Amsterdam: Elsevier; 1989. p. 393.
- [7] Bourne NK. *Proc Roy Soc Lond A* 2002;458:1999.
- [8] Grady DE. *J Phys IV* 1994;4:C8.
- [9] Chen M, McCauley JW, Hemker KJ. *Science* 2003;299:1563.
- [10] Fischer-Cripps AC. *Vacuum* 2000;58:569.
- [11] Domnich V, Gogotsi Y, Trenary M. *Mater Res Soc Symp Proc* 2001;649:Q8.9.1.
- [12] Fischer-Cripps AC. *J Mater Res* 2001;16:1579.
- [13] Hay JL, Pharr GM. Instrumented indentation testing. In: Kuhn H, Medlin D, editors. *Mechanical testing and evaluation*, vol. 8. Materials Park, OH: ASM International; 2000. p. 232.
- [14] Gogotsi Y, Domnich V. *High-pressure surface science and engineering*. Bristol and Philadelphia: Institute of Physics Publishing; 2004. p. 639.
- [15] Gilman JJ. *Philos Mag B* 1993;67:207.
- [16] Blank VD, Kulnitskiy BA. *High Pressure Res* 1996;15:31.
- [17] Domnich V, Gogotsi Y, Trenary M, Tanaka T. *Appl Phys Lett* 2002;81:3783.
- [18] Manghnani M. Elastic and vibrational properties of hard and superhard materials under high pressure. Presented at the PAC RIM 4 Conference in Maui, Hawaii, 2001; paper PAC6-B-10-2001.
- [19] Page TF, Oliver WC, McHargue CJ. *J Mater Res* 1992;7:450.
- [20] Hainsworth SV, Whitehead AJ, Page TF. The nanoindentation response of silicon and related structurally similar materials. In: Bradt RC, Brookes CA, Routbort JL, editors. *Plastic deformation of ceramics*. New York: Plenum Press; 1995. p. 173.
- [21] Page TF, Riester L, Hainsworth SV. *Mater Res Soc Symp Proc* 1998;522:113.
- [22] Nowak R, Sekino T, Niihara K. *Acta Mater* 1999;47:4329.
- [23] Weppelmann ER, Field JS, Swain MV. *J Mater Res* 1993;8: 830.
- [24] Gogotsi YG, Domnich V, Dub SN, Kailer A, Nickel KG. *J Mater Res* 2000;15:871.
- [25] Domnich V, Gogotsi Y, Dub S. *Appl Phys Lett* 2000;76:2214.
- [26] Ge D, Domnich V, Gogotsi Y. *J Appl Phys* 2003;93:2418.
- [27] Ge D, Domnich V, Gogotsi Y. *J Appl Phys* 2004;95:2725.
- [28] Minor AM, Morris Jr JW. *Appl Phys Lett* 2001;79:1625.
- [29] Shirai K, Emura S. *J Phys: Condens Matter* 1996;8:10919.
- [30] Aselage TL, Tallant DR, Emin D. *Phys Rev B* 1997;56:3122.
- [31] Werheit H, Schmechel R, Kuhlmann U, Kampen TU, Mönch W, Rau A. *J Alloys Compd* 1999;291:28.
- [32] Lazzari R, Vast N, Besson JM, Baroni S, Dal Corso A. *Phys Rev Lett* 1999;83:3230.
- [33] Ferrari AC, Robertson J. *Phys Rev B* 2000;61:14095.
- [34] Dresselhaus MS, Dresselhaus G, Pimenta MA, Eklund PC. Raman scattering in carbon materials. In: Pelletier M, editor. *Analytical applications of Raman spectroscopy*. Oxford, UK: Blackwell Science; 1999. p. 367.
- [35] Saka H, Shimatani A, Suganuma M, Suprijadi. *Philos Mag A* 2002;82:1971.
- [36] Tachi M, Suprijadi, Arai S, Saka H. *Philos Mag Lett* 2002;82: 133.
- [37] Gogotsi YG, Kailer A, Nickel KG. *Mater Res Innov* 1997;1:3.
- [38] Aselage TL, Emin D. Structural model of the boron carbide solid solution. In: *Boron-rich solids*. American Institute of Physics; 1991. p. 177.
- [39] Zeuch DH, Montgomery ST, Holcomb DJ. *J Mater Res* 1999;14:1814.
- [40] Crain J, Ackland GJ, Maclean JR, Piltz RO, Hatton PD, Pawley GS. *Phys Rev B* 1994;50:13043.
- [41] Oliveira JC, Paiva P, Oliveira MN, Conde O. *Appl Surf Sci* 1999;138–139:159.